Earth and Planetary Science Letters 394 (2014) 70–81

Contents lists available at ScienceDirect

Earth and Planetary Science Letters

www.elsevier.com/locate/epsl

Persistent environmental change after the Paleocene–Eocene Thermal Maximum in the eastern North Atlantic

André Bornemann [a,*], Richard D. Norris [b], Johnnie A. Lyman [b], Simon D'haenens [c], Jeroen Groeneveld [d], Ursula Röhl [e], Kenneth A. Farley [f], Robert P. Speijer [c]

[a] Intitut für Geophysik und Geologie, Universität Leipzig, Germany
[b] Scripps Institution of Oceanography, University of California, San Diego, CA, USA
[c] Department of Earth and Environmental Sciences, KU Leuven, Belgium
[d] Fachbereich für Geowissenschaften, Universität Bremen, Germany
[e] MARUM – Zentrum für Marine Umweltwissenschaften, Universität Bremen, Germany
[f] Division of Geological and Planetary Sciences, California Institute of Technology, Pasadena, CA, USA

ARTICLE INFO

Article history:
Received 16 July 2013
Received in revised form 4 March 2014
Accepted 10 March 2014
Available online xxxx
Editor: J. Lynch-Stieglitz

Keywords:
PETM
carbon isotope excursion
paleoclimatology
paleoceanography
isotope geochemistry

ABSTRACT

The Paleocene–Eocene Thermal Maximum (PETM; ~56 Ma) is associated with abrupt climate change, carbon cycle perturbation, ocean acidification, as well as biogeographic shifts in marine and terrestrial biota that were largely reversed as the climatic transient waned. We report a clear exception to the behavior of the PETM as a reversing climatic transient in the eastern North Atlantic (Deep-Sea Drilling Project Site 401, Bay of Biscay) where the PETM initiates a greatly prolonged environmental change compared to other places on Earth where records exist. The observed environmental perturbation extended well past the $\delta^{13}C$ recovery phase and up to 650 kyr after the PETM onset according to our extraterrestrial ^{3}He-based age-model. We observe a strong decoupling of planktic foraminiferal $\delta^{18}O$ and Mg/Ca values during the PETM $\delta^{13}C$ recovery phase, which in combination with results from helium isotopes and clay mineralogy, suggests that the PETM triggered a hydrologic change in western Europe that increased freshwater flux and the delivery of weathering products to the eastern North Atlantic. This state change persisted long after the carbon-cycle perturbation had stopped. We hypothesize that either long-lived continental drainage patterns were altered by enhanced hydrological cycling induced by the PETM, or alternatively that the climate system in the hinterland area of Site 401 was forced into a new climate state that was not easily reversed in the aftermath of the PETM.

1. Introduction

The Paleocene–Eocene Thermal Maximum (PETM; ~56 Ma) is the most prominent of a number of global transient warming events punctuating early Paleogene warmth. It is characterized by (i) a short-lived 170–230 kyr long, negative $\delta^{13}C$ excursion of 1‰ to 8‰ in marine and terrestrial archives (e.g., McInerney and Wing, 2011; Murphy et al., 2010; Röhl et al., 2007), (ii) warming of bottom and surface water by several degrees Celsius (e.g., Kennett and Stott, 1991; Tripati and Elderfield, 2005), (iii) a decrease of $CaCO_3$ in deep-sea sediments related to lysocline shallowing and ocean acidification (e.g., Ridgwell and Schmidt, 2010; Zachos et al., 2005), and (iv) a major extinction of deep-sea benthic foraminifera and a turnover of the calcareous plankton communities (e.g., Gibbs et al., 2006; Kelly et al., 1996; Speijer et al., 2012; Thomas, 2007).

The strong negative PETM carbon isotope excursion (CIE) indicates that – depending on the isotopic composition of the carbon source – 2000 to 12 000 Gt of isotopically light carbon was added to the global carbon cycle within less than 20 kyr (Dickens, 2011). Potential carbon sources include CO_2 from oxidized organic matter or the dissociation of methane derived from gas hydrates (Dickens, 2011), the release of thermogenic methane during the emplacement of the North Atlantic Igneous Province (Svensen et al., 2004), and thawing of permafrost (DeConto et al., 2012).

The PETM warming under high pCO_2 conditions caused an intensification of the hydrological cycle as is evident in many places worldwide and documented by a high seasonality in precipitation, enhanced river discharge, associated sedimentary mass movements

* Corresponding author. Tel.: +49 341 9732903.
E-mail address: a.bornemann@uni-leipzig.de (A. Bornemann).

http://dx.doi.org/10.1016/j.epsl.2014.03.017
0012-821X/

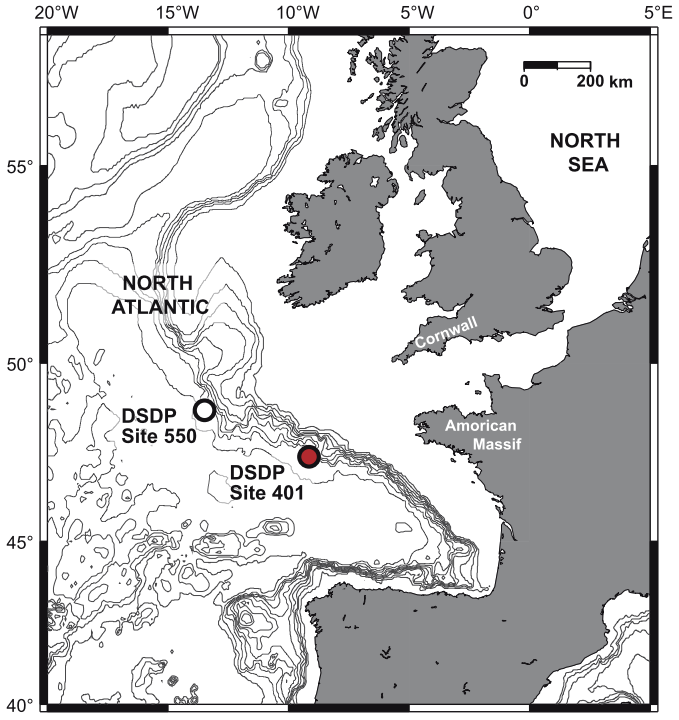

Fig. 1. Geographic map of the eastern North Atlantic showing the position of DSDP Sites 401 and 550.

and an increase of terrestrial input into the oceans (Bowen et al., 2004; Kelly et al., 2005; McInerney and Wing, 2011; Pagani et al., 2006; Schmitz and Pujalte, 2007; Sluijs et al., 2007a, and references therein). The existence of this weathering response is well known, but its geographic variability is still poorly understood, even for the circum-North Atlantic region from where numerous data sets exist so far (e.g., Dypvik et al., 2011; John et al., 2008, 2012; Kender et al., 2012; Schmitz and Pujalte, 2003). However, many of these records are either incomplete or did not tie the terrestrial response to the deep-marine signal. Moreover, detailed PETM deep-sea records based on both well-preserved planktic and benthic foraminifera from the northern hemisphere are generally rare.

Here we report new geochemical data from the PETM in Deep Sea Drilling Project (DSDP) Site 401, which is situated in the outer Bay of Biscay (eastern North Atlantic, Fig. 1). There, the PETM consists of an extended, overall clay-rich succession containing well-preserved foraminiferal tests (Fig. 2) allowing for a detailed geochemical study of foraminifera calcite. We used monospecific $\delta^{13}C$, $\delta^{18}O$ and Mg/Ca records of benthic, subsurface and surface dwelling foraminifera to investigate how the entire water column was affected by the PETM. In addition, the existence of the thick clay-rich PETM interval allows linkages with both continental signals and a deep-marine record. In order to achieve this we further employed helium isotopes to unravel mass accumulation rates (Farley and Eltgroth, 2003; Murphy et al., 2010) and clay mineralogy to constrain the continental response to the PETM.

2. Material and methods

2.1. Material

DSDP Site 401 (47°25.65′N, 08°48.62′W, 2495 m water depth) is located on the Meriadzek Terrace on the northern margin of the Bay of Biscay, eastern North Atlantic (Montadert et al., 1979). In the early Paleogene, this site was located at ~42°32′N and 10°25′W (McInerney and Wing, 2011). The paleo-water depth has been estimated at 1.8–2 km based on benthic foraminifera (D'haenens et al., 2012).

The study interval (192.4–204.2 mbsf) comprises two cores (Cores 13 and 14) separated by a 2.1-m-wide coring gap (Fig. 3). Lithologically, these cores can be separated into three units: (i) the pre-PETM interval of Core 14 (below 202.51 mbsf) is made up by calcareous nannofossil chalks of grayish-orange color, (ii) a clay-rich unit (194.7–202.51 mbsf) consisting of yellowish brown marls and covering parts of both cores including the PETM at its base, and (iii) above (in Core 13), grayish-orange calcareous nannofossil chalks occur again (Fig. 3). Wireline-logs (Montadert et al., 1979 Fig. S1) show that the clayey succession is continuous without any major lithological change in the recovery gap between the two studied cores, and confirm that the coring gap is indeed 2.1-m-wide.

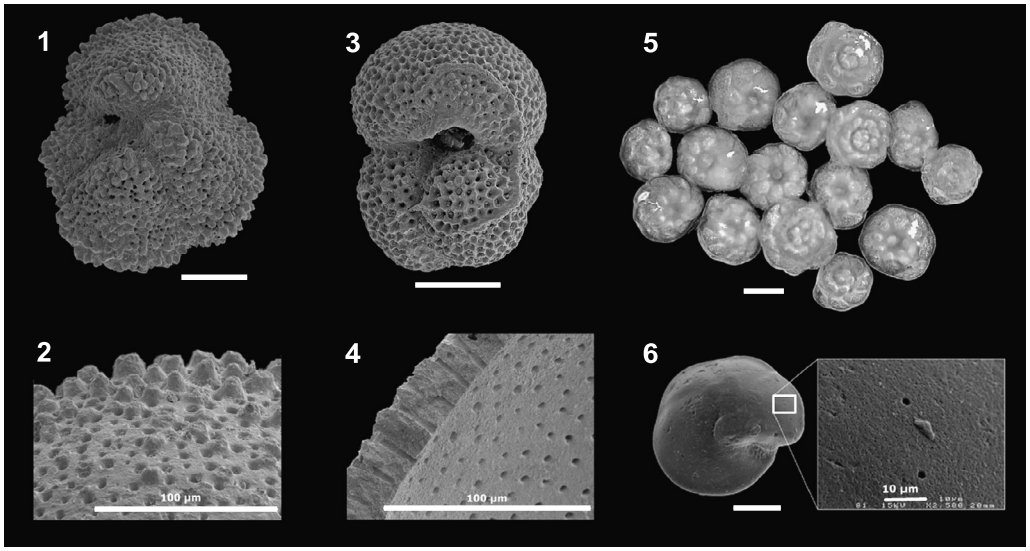

Fig. 2. Scanning electron and light microscope images to display the state of preservation of taxa studied herein. Foraminiferal tests are unusually well preserved and display no indications of dissolution and/or recrystallization. (1) *Morozovella subbotinae*, (2) close up of *Acarinina soldadoensis*, (3) *Subbotina patagonica*, (4) wall ultrastructure of *S. patagonica*, (5) *Nuttallides truempyi*, (6) *Oridorsalis umbonatus* with close up (scale bar = 100 µm, if not stated different).

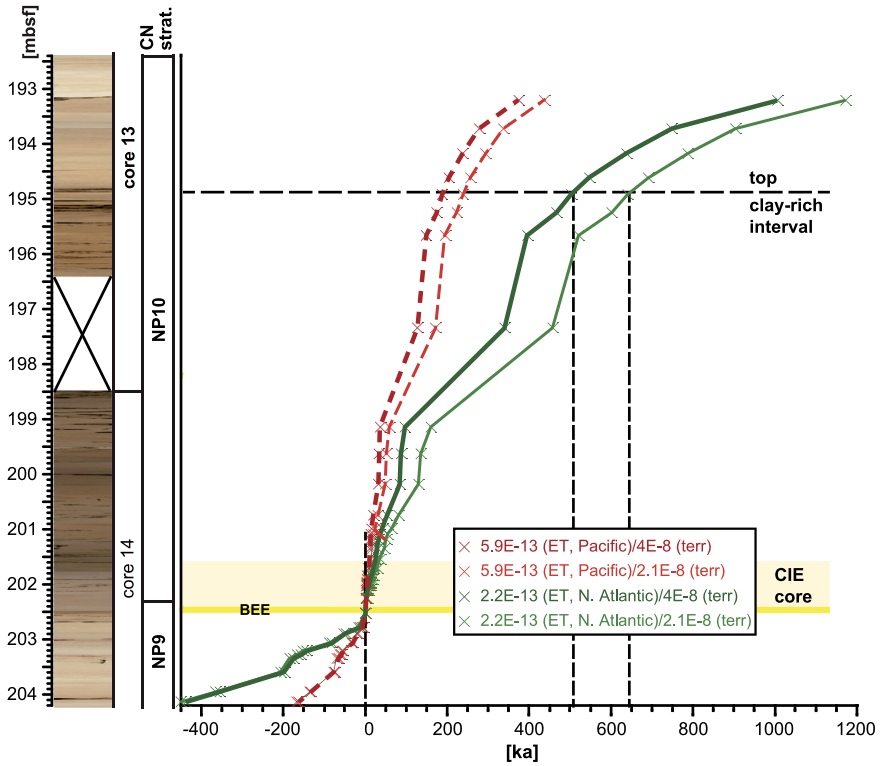

Fig. 3. Lithology, calcareous nannofossil (CN) biostratigraphy and extraterrestrial ^{3}He-based age models. Due to the lack of a calibration interval for estimating the extraterrestrial ^{3}He flux, we calculated relative ages with respect to the onset of the PETM (55.96 Ma, Vandenberghe et al., 2012) CIE at 202.51 mbsf by assuming two endmembers for the extraterrestrial (ET) ^{3}He flux (2.2E−13 and 5.9E−13 cm^{3} STP cm^{-2} kyr^{-1}, see also method part) as well as for two terrestrial (terr.) ^{3}He/^{4}He endmembers (2.1E−8 and 4E−8). Note that the marked data points represent mid-points between analyzed sediment samples. BEE: benthic foraminiferal extinction event. (For interpretation of the references to color in this figure, the reader is referred to the web version of this article.)

2.2. Sediment geochemistry

For X-ray fluorescence (XRF) core scanning, the split core surface was covered with a 4 µm thin SPEXCerti Prep Ultralene foil to avoid contamination of the XRF measurement unit and desiccation of the sediment. Data were collected every 1 cm down-core over a 1 cm^{2} area with down-core slit size of 10 mm using generator settings of 10 kV, a current of 500 µA, and a sampling time of 10 s directly at the split core surface of the archive half with XRF Core Scanner III (AVAATECH Serial No. 12) at the MARUM, Bremen. The data reported here were acquired by a Canberra X-PIPS Detector (Model SXP 5C – 200 – 1500 V2) with 200 eV X-ray resolution, the Canberra Digital Spectrum Analyzer DAS 1000, and an Oxford Instruments 50 W XTF5011 X-Ray tube with Rh target material. Raw data spectra were processed using the X-ray spectra by Iterative Least square software (WIN AXIL) package from Canberra Eurisys. The clayey interval shows a large number of cracks which result in negative outliers with very low intensities. A few of these outliers that could be easily identified on core photos were manually removed from the data set shown in Figs. 4 and 7C.

Bulk sediment samples were analyzed for $CaCO_3$ content employing the carbonate bomb technique (Müller and Gastner, 1971). The precision for replicate analyses is 2 wt%. Additional $CaCO_3$ data were derived from the decalcification process for He isotope analyses (Murphy et al., 2010).

2.3. X-ray diffractometry (XRD)

Selected sediment samples were studied for clay mineralogy (<2 µm). Sample preparation and analysis followed standard procedures described by Ehrmann et al. (1992) and Petschick et al. (1996). Carbonate-free clay samples were mounted as texturally oriented aggregates and measured by XRD (CoKα radiation) in the range from 2° to 40° 2Θ at 0.02° steps using a Rigaku MiniFlex (Universität Leipzig). For discrimination of kaolinite and chlorite the (002) peak of kaolinite at 3.58 Å and the (004) peak of chlorite at 3.54 Å were analyzed. Peak areas were measured using the MacDiff software package. The calculation of relative abundances of common clay minerals follows Biscaye (1965).

2.4. Helium isotopes and age model

Preparation for He isotopes followed methods described by Farley and Eltgroth (2003) and Patterson and Farley (1998). This included freeze-drying, homogenization via agate mortar and pestle, and decarbonation with 10% acetic acid solution of ~1.5 g samples. The residue containing all the He, was isolated by centrifugation, transferred to a tin sample cup, and baked to 90 °C to remove adsorbed water. Helium was extracted from the sample by heating to 1300 °C. It was purified of active gases and other noble gases, cryo-concentrated, and analyzed on an MAP215-50 noble gas mass spectrometer at the California Institute of Technology following standard procedures (Patterson and Farley, 1998). In all cases blank corrections were <10% for both isotopes. Typical analytical precision is better than 5% for ^{3}He and 3% for ^{4}He. Helium in marine sediment is a two-component mixture of relatively light extraterrestrial and heavy terrestrial helium. To determine the fraction of ^{3}He attributable to an extraterrestrial source and ^{4}He to a terrigenous origin we used a standard two-component mixing model (Farley and Mukhopadhyay, 2001).

The terrestrial endmembers for ^{3}He/^{4}He are highly variable and the source of terrestrial material may change through time, whereas the extraterrestrial composition, dominantly solar wind ions, is likely to be constant over geological timescales (Mukhopadhyay et al., 2001). We, thus, explored the use of two

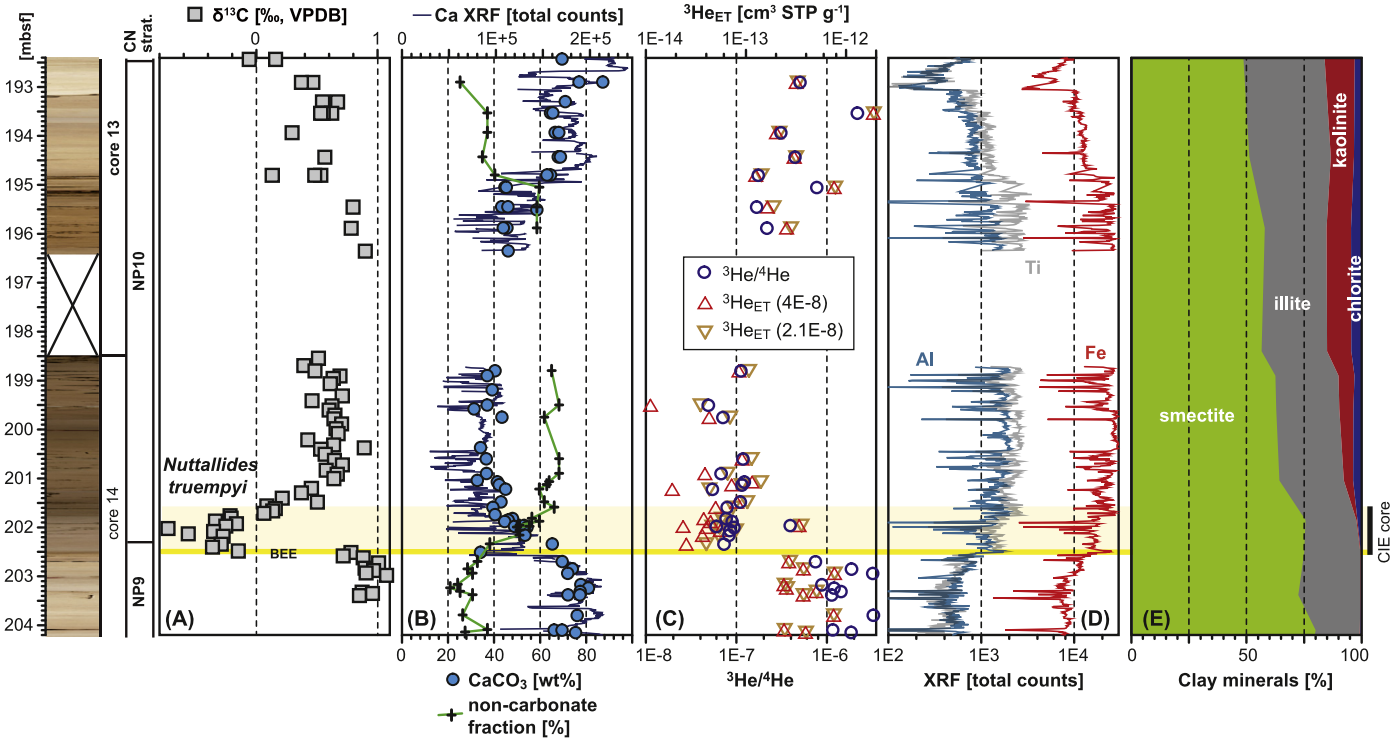

Fig. 4. Lithology, calcareous nannofossil (CN) biostratigraphy and geochemical data from the PETM interval at DSDP Site 401, Cores 13 and 14. (A) $\delta^{13}C$ record of the benthic foraminifer *Nuttallides truempyi* for chemostratigraphy. (B) $CaCO_3$ data from discrete samples, XRF core scanning Ca intensities, and the non-carbonate fraction (NCF) determined during He isotope analyses. (C) Results from helium isotope analyses: $^3He/^4He$, and extraterrestrial $^3He_{ET}$ for two terrestrial $^3He/^4He$ endmembers, (D) XRF core scanning intensities of Al (blue), Ti (gray) and Fe (red), (E) relative clay mineral abundances. (For interpretation of the references to color in this figure legend, the reader is referred to the web version of this article.)

different terrestrial endmembers ($^3He/^4He$ of 2.1E−8 and 4E−8). A $^3He/^4He$ of 2.41E−4 was assumed for the extraterrestrial endmember.

For the He-based age model and for calculation of terrigenous ^4He mass accumulation rates (MAR) we require knowledge of the local extraterrestrial ^3He ($^3He_{ET}$) flux. In the absence of a suitable calibration interval at our site, we used the $^3He_{ET}$ flux of 5.91E−13 cm^3 STP cm^{-2} ky^{-1} for the central Pacific (Marcantonio et al., 2009) and 2.2E−13 cm^3 STP cm^{-2} ky^{-1} for the North Atlantic region (Farley and Eltgroth, 2003) as endmembers. These endmembers cover nearly the entire range of values published for the Paleocene–Eocene boundary interval so far. The value from the Pacific is well in line with another one published by Farley (1995) of ~5E−13 cm^3 STP cm^{-2} ky^{-1} and the North Atlantic value from ODP Site 1051 of 2.2E−13 cm^3 STP cm^{-2} ky^{-1} (Farley and Eltgroth, 2003) is close to one from Italy (~1.9E−13 cm^3 STP cm^{-2} ky^{-1}, Mukhopadhyay et al., 2001). Thus, these endmember values are well substantiated. We note that the most recent flux estimated for this time interval, from Walvis Ridge, lies between these two values (3.7E−13 cm^3 STP cm^{-2} ky^{-1}, Murphy et al., 2010). For calculation of the relative ages with respect to the CIE onset shown in Fig. 3, we followed Farley and Eltgroth (2003).

2.5. Foraminiferal test chemistry ($\delta^{13}C$, $\delta^{18}O$, Mg/Ca)

We generated stable isotope ($\delta^{13}C$, $\delta^{18}O$) and Mg/Ca records of planktic and benthic foraminifera. Bottom water conditions were estimated from $\delta^{18}O$ analyses of epibenthic *Nuttallides truempyi* (most data are from Nunes and Norris, 2006) while Mg/Ca analyses were based upon the shallow endobenthic species *Oridorsalis umbonatus*. Subsurface conditions are inferred from analyses of *Subbotina patagonica*, while surface water conditions were determined using the photosymbiont-bearing *Acarinina soldadoensis* (isotopes only) and *Morozovella subbotinae*. For foraminiferal studies, samples were dried at ~50 °C, weighed, soaked in tap water for 24 hours, gently washed under running water through a 63-μm-sieve, dried and weighed again. For $\delta^{13}C$ and $\delta^{18}O$ analyses planktic foraminifera were picked from the 250–350 μm size fraction and measured using a Caroussel-48 automatic carbonate preparation device coupled to a Finnigan MAT252 mass spectrometer at Scripps Institution of Oceanography and a Kiel III online carbonate preparation line connected to a ThermoFinnigan 252 mass spectrometer at the Universität Erlangen. All values are reported in ‰ relative to V-PDB by assigning a $\delta^{13}C$ value of +1.95‰ and a $\delta^{18}O$ value of −2.2‰ to NBS19. Reproducibility was checked by replicate analyses of laboratory standards and is better than ±0.04‰ and ±0.07‰ (1σ) for $\delta^{13}C$ and $\delta^{18}O$, respectively, in both laboratories. Repeated measurements of the same taxa and sample are similar to these deviations (~0.1‰) for both $\delta^{13}C$ and $\delta^{18}O$. In order to estimate absolute temperatures we applied the Erez and Luz (1982) equation to planktic foraminifera and Shackleton (1974) to the benthic foraminifer *N. truempyi*. We assumed seawater $\delta^{18}O$ values of −0.4‰ SMOW for surface waters which is well in line with modeling results of Huber et al. (2003) and Tindall et al. (2010), and −0.97‰ SMOW for thermocline and bottom waters according to Zachos et al. (1994) for nearly ice-free conditions.

For Mg/Ca, ~20 specimens per species and sample were picked and gently crushed from the 250 to 450 μm size fraction. Sample cleaning followed Barker et al. (2003), which consisted of five water and two methanol washes followed by two oxidation steps for 10 min each (with 1% NaOH-buffered H_2O_2), and a weak acid leach (0.001 M QD HNO_3) before dissolving the foraminiferal calcite into 0.075 M QD HNO_3. The solutions were centrifuged (10 min at 6000 rpm), transferred into test tubes and diluted. Mg/Ca was measured using a Perkin Elmer Optima 3300R ICP-

OES equipped with an auto sampler and an ultrasonic nebulizer U-5000AT (Cetac Technologies Inc.) housed at the Faculty of Geosciences, University of Bremen. The Mg/Ca values are reported as mmol mol^{-1}. Relative standard deviation of the external standard was ±0.08% and the drift over a typical analytical session of 24 h was ±0.67%. Analytical precision of the samples was ±0.09% ($n = 52$) and long-term reproducibility of foraminiferal samples ($n = 72$) ± 0.11 mmol mol^{-1} (±3.43%). Mg/Ca temperatures are based on Elderfield and Ganssen (2000) for planktic foraminifera and Rathmann and Kuhnert (2008) for *O. umbonatus*. Since there are a number of uncertainties for absolute temperatures (Lear et al., 2000) — including divergent temperature calibrations for Mg/Ca, and for the seawater composition of both δ^{18}O and Mg/Ca — we primarily focus on relative temperature changes, which are largely independent of these issues. Influence of severe, punctuated $CaCO_3$ dissolution during the PETM on the oceanic Ca budget and, thus, on seawater Mg/Ca can be considered to be insignificant according to calculations by Komar and Zeebe (2011). Moreover, both cation species are conservative having oceanic residence times that are much longer than the interval studied herein (Broecker and Peng, 1982).

3. Results and discussion

3.1. Age control

Biostratigraphically, the studied cores cover the topmost part of calcareous nannofossil zone NP9 and the entire NP10 (base 55.86 Ma, top 54.17 Ma, Vandenberghe et al., 2012), with the NP9–NP10 boundary positioned 20 cm above the onset of the CIE (202.3 mbsf; Fig. 3) and the NP10–NP11 boundary at the top of the study interval (192.43 mbsf). We further identified the benthic foraminiferal extinction event (Thomas, 2007, Fig. 3) at 202.51 mbsf.

A chemostratigraphic control for the PETM interval exists due to the characteristic shape of the benthic foraminiferal δ^{13}C record with a CIE core interval covering the onset of the CIE (202.51 mbsf), its peak interval with sustained negative values (202.48–201.65 mbsf), an early recovery phase (201.65–201.2 mbsf; see also Fig. 4A), and the subsequent recovery phase lasting until δ^{13}C nearly returns to pre-event values. The duration of these phases are rather variable depending on the method applied and the type of archive, and is still a matter of debate (Röhl et al., 2007; McInerney and Wing, 2011). Indeed, the values for the CIE core interval from the well-calibrated ODP Site 1266 (Walvis Ridge) vary between 66 kyr (cyclostratigraphy, Röhl et al., 2007) and 113 kyr (^{3}He$_{ET}$ calibration, Murphy et al., 2010).

Additional high-resolution age control is hampered by the lack of a sophisticated cyclostratigraphy for the PETM interval of DSDP Site 401, because Site 401 consists of a single hole record and has recovery gaps between adjacent cores (Fig. 3) in combination with the lack of distinct cycles in intervals of the recovered core. Thus, we applied an ^{3}He$_{ET}$-based age model for the studied cores covering the PETM interval (Fig. 3). Compared to previous work (e.g., Murphy et al., 2010) the model provides only a limited precision estimate for the duration of the PETM due to (i) the high amounts of terrestrial He at this site (Fig. 4D), and (ii) the spatial variability in extraterrestrial ^{3}He$_{ET}$ flux that could not be locally calibrated, because of the lack of a stratigraphically well-defined calibration interval.

Based on our ^{3}He$_{ET}$ age-model, the entire clay-rich sequence at Site 401 (from 202.5–194.9 mbsf) covers between 200 and 650 kyr (Fig. 3). However, there are a number of arguments suggesting that the upper limit of our age-model is likely to be the more realistic estimate. If we choose to calibrate our ^{3}He$_{ET}$ age-model using the ^{3}He$_{ET}$ flux for the Pacific (Marcantonio et al., 2009), the estimated duration of the CIE core is much too short (~10 kyr), whereas this interval has been estimated to have a duration at least six-times longer (66–113 kyr; Murphy et al., 2010; Röhl et al., 2007). Use of the Pacific ^{3}He$_{ET}$ flux in our age model would imply that the entire sequence between ~195 and 202.5 mbsf represents the PETM as conventionally-recognized, but this finding is not only contradicted by the δ^{13}C record (which confines the CIE core to the interval ~201.5–202.5 mbsf), but would also require a very high average sedimentation rate of ~3.7 cm kyr^{-1}, compared to typical pelagic sedimentation rates in the Paleocene of <1 cm kyr^{-1} as obtained by using the ^{3}He$_{ET}$ flux value from the Atlantic. In contrast, calibration based upon the estimates of the North Atlantic (Farley and Eltgroth, 2003) and Italy (Mukhopadhyay et al., 2001) ^{3}He$_{ET}$ flux places the top of the clay-rich horizon at ~500–650 kyr above the base of the CIE (Fig. 3). This age range agrees with a chemostratigraphic correlation between Site 401 and nearby ODP Site 550 (Fig. 5) which suggests that the dark lithological level ~195 mbsf correlates to the "F" level of Cramer et al. (2003) that is dated at 750 kyr (Zachos et al., 2010) after the PETM onset. Our correlation of Site 401 and Site 550 matches also an earlier lithological correlation by Knox (1985) for the early Eocene of the same two sites. Furthermore, a tie at the "F" level between Site 401 and Site 550 also makes sense in terms of the sequence of two younger key horizons (such as "G" and "H1") in the XRF records and the δ^{13}C data of both benthic foraminifera and bulk carbonate (Fig. 5). We conclude that deposition of the clay-rich interval persisted between 300 and 450 kyr after the termination of the PETM.

3.2. Carbonate content

The onset of the PETM at DSDP Site 401 is characterized by a prominent drop in $CaCO_3$ from 80 to 30 wt%, also expressed by an increase of the non-carbonate fraction and in great detail by the Ca intensity data from XRF core scanning (Fig. 4B). According to a numerical dilution-dissolution model (Fig. 6) of Zeebe and Zachos (2007), this decrease in $CaCO_3$ can be explained by a ~9-fold increase in clay supply. This increase in clay flux assumes the absence of severe carbonate dissolution as is evident from our micropaleontological and geochemical findings (see below).

Unlike observations at several other deep-sea sites, moderate $CaCO_3$ values of 40 wt% to 50 wt% persist well past the end of the CIE core and never reach zero (Fig. 4B). In fact, the entire asymptotic δ^{13}C recovery is characterized by clayey brown marls, and high carbonate values (~70–80%) are not re-established until ~650 kyr after the onset of the PETM (at ~195 mbsf). Despite the persistence of moderate $CaCO_3$ values, foraminifer preservation is unusually good (Nunes and Norris, 2006). The lack of severe dissolution at the base of the CIE is also supported by nannofossil smear slide studies based on tooth-pick samples from all lithologies of this particular interval. Indeed, the high quality of microfossil preservation (Fig. 2) suggests that Site 401 did not experience as much lysocline shallowing as observed in the South Atlantic and Pacific oceans (Colosimo et al., 2006; Zachos et al., 2005). This conclusion is compatible with a proposed deep-water circulation switch (Nunes and Norris, 2006) during the PETM from a southern ocean source to a North Atlantic source. A North Atlantic source would be younger and less saturated with CO_2, and, thus, able to explain the lack of dissolution at DSDP Site 401, and to store more carbon than older, more saturated southern ocean waters.

3.3. Carbon isotope excursion (CIE)

At DSDP Site 401 all three foraminifera species display a negative δ^{13}C excursion of ~2‰ at the start of the PETM followed

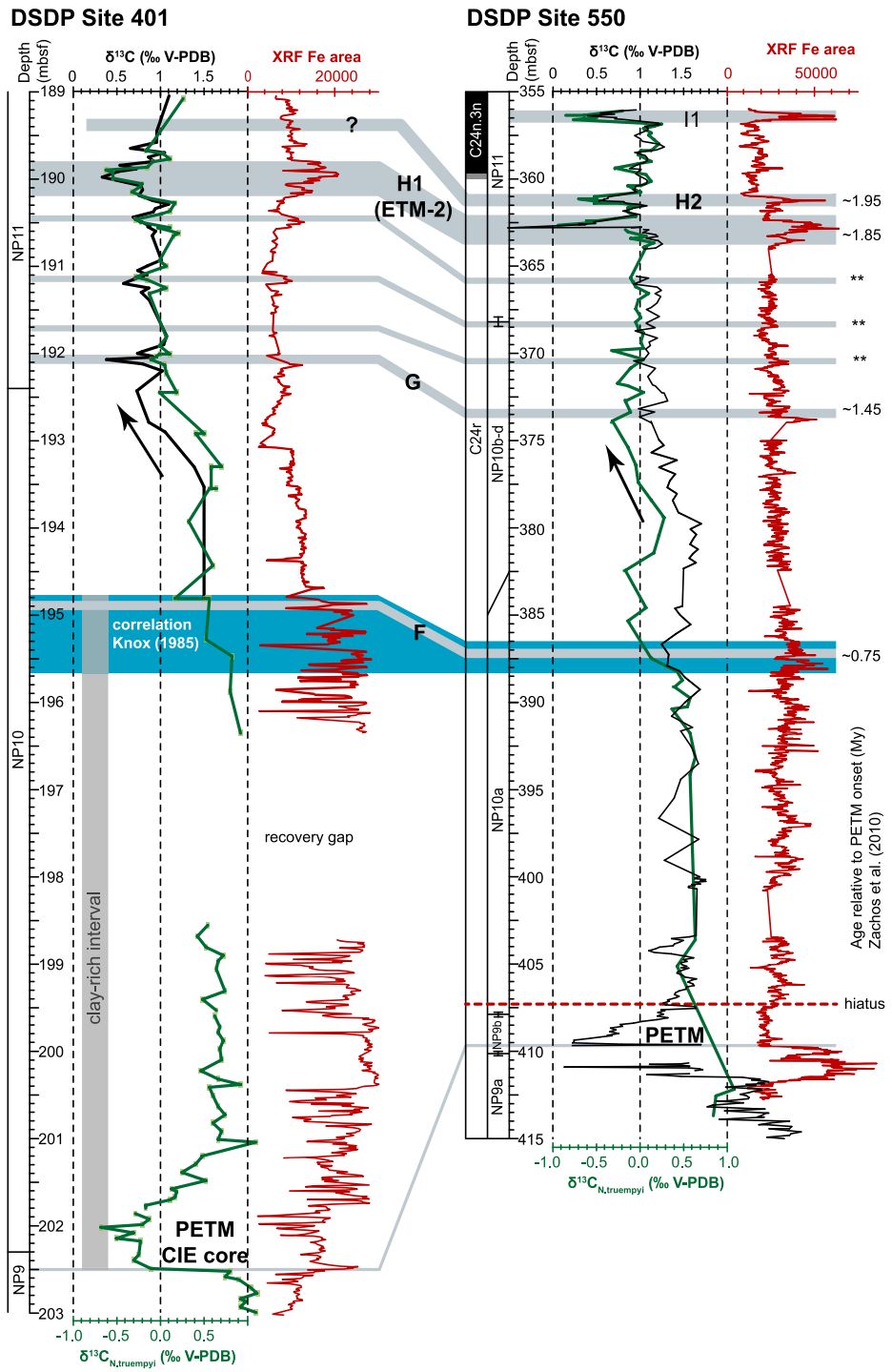

Fig. 5. Chemostratigraphic correlation between DSDP Site 401 (this paper) and DSDP Site 550. Data shown here are based on our work, Cramer et al. (2003), Raffi et al. (2005), Westerhold and Röhl (2009) and D'haenens et al. (2012, pers. comm.). The correlation suggests that the dark lithological level ~195 mbsf correlates to the "F" level (Cramer et al., 2003), and this correlation is supported by similar correlations to levels "G" and "H1" as well as the general pattern of the $\delta^{13}C$ stratigraphy. An earlier correlation by Knox (1985) is highlighted in blue for the early Eocene of the same two sites. The "F" level is dated to be 750 kyr younger than the onset of the PETM (Zachos et al., 2010) and is, thus, of a similar order of relative age as the 500–650 kyr of our age model based upon the Atlantic extraterrestrial ^{3}He flux. (For interpretation of the references to color in this figure legend, the reader is referred to the web version of this article.)

by a synchronous recovery (Fig. 7A). Surface dwelling taxa show a slightly higher amplitude of the $\delta^{13}C$ excursion (>2‰ for *Acarinina soldadoensis*) and a more rapid recovery after the CIE (*Morozovella subbotinae*), and generally heavier $\delta^{13}C$ values (~2 to 4‰) than thermocline (*Subbotina patagonica*, −1 to 2.3‰) and benthic (*Nuttallides truempyi*, −0.8 to 1‰) species (Fig. 7A). The $\delta^{13}C$ differences between the depth habitats follow the typical vertical oceanic $\delta^{13}C_{DIC}$ gradient (Kroopnick, 1985), whereas differences between surface and sub-surface dwelling taxa might be also due to the different behavior of photosymbionts that strongly control the $\delta^{13}C$ values in surface dwelling planktic foraminiferal calcite in response to PETM stress conditions (Edgar et al., 2012;

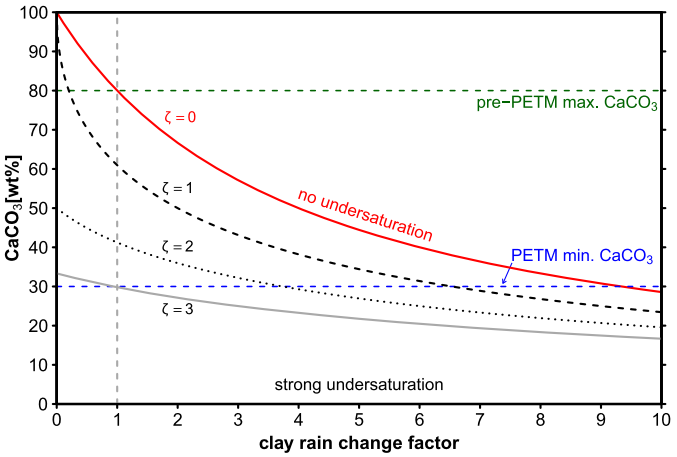

Fig. 6. Sedimentary $CaCO_3$ wt% as a function clay supply and different degrees of carbonate undersaturation (ζ, normalized to $CaCO_3$ rain, see details in Zeebe and Zachos, 2007). Applying this numerical dilution-dissolution model for Site 401 the shift from 80 wt% $CaCO_3$ (pre-PETM) to a minimum PETM value of 30 wt% is well in line with a ~9-fold increase in clay supply and, thus, of similar magnitude as the observed increase in terrigenous ^{4}He, in absence of severe dissolution ($\zeta = 0$) as is evident from our micropaleontological and geochemical findings.

Norris, 1996). In addition, at the base of the CIE both planktic foraminifera taxa *S. patagonica* and *M. subbotinae* show in one sample very negative δ^{13}C values suggesting a larger initial negative CIE amplitude of about 3‰.

The general shape of the CIE at DSDP Site 401 is very similar to that from other deep-sea sites, but the observed amplitude of ~2‰ is smaller than is usually seen in the deep-sea, where excursions of >2.5‰ are more typical. For the benthic record Nunes and Norris (2006) attributed this difference in the amplitude of the CIE to a change in the location of deep water overturning during the PETM that changed the 'age' and $\delta^{13}C_{DIC}$ of waters in the NE Atlantic. This scenario has been intensively discussed over the last years, but so far, numerical models provide no consistent picture for the deep-sea circulation in the North Atlantic (Lunt et al., 2010; Winguth et al., 2012).

An alternative explanation for the relatively small δ^{13}C excursion would be that the CIE is incomplete (McCarren et al., 2008). The strong negative δ^{13}C values for planktic foraminifera (Fig. 7A) at the base of the CIE could support this explanation since they suggest that the CIE briefly attained a δ^{13}C excursion similar that observed in other deep-sea sites. We note that the shape and magnitude of the Site 401 δ^{13}C excursion is very similar to that of the Forada section in Italy (Giusberti et al., 2007) in which there is an initial negative δ^{13}C excursion of 3‰, followed by a "plateau" where δ^{13}C is about 2‰ more negative than pre-PETM values through the core of the CIE. The Forada PETM record is considered to be complete, because the CIE interval covers the maximum number of precessional cycles (Röhl et al., 2007). Moreover, dissolution has not been observed at Site 401, neither in the studied sediment samples nor in the XRF core scanning Ca data. In conclusion, we consider the CIE interval at DSDP Site 401 as largely complete, although we cannot fully rule out that the CIE is truncated at

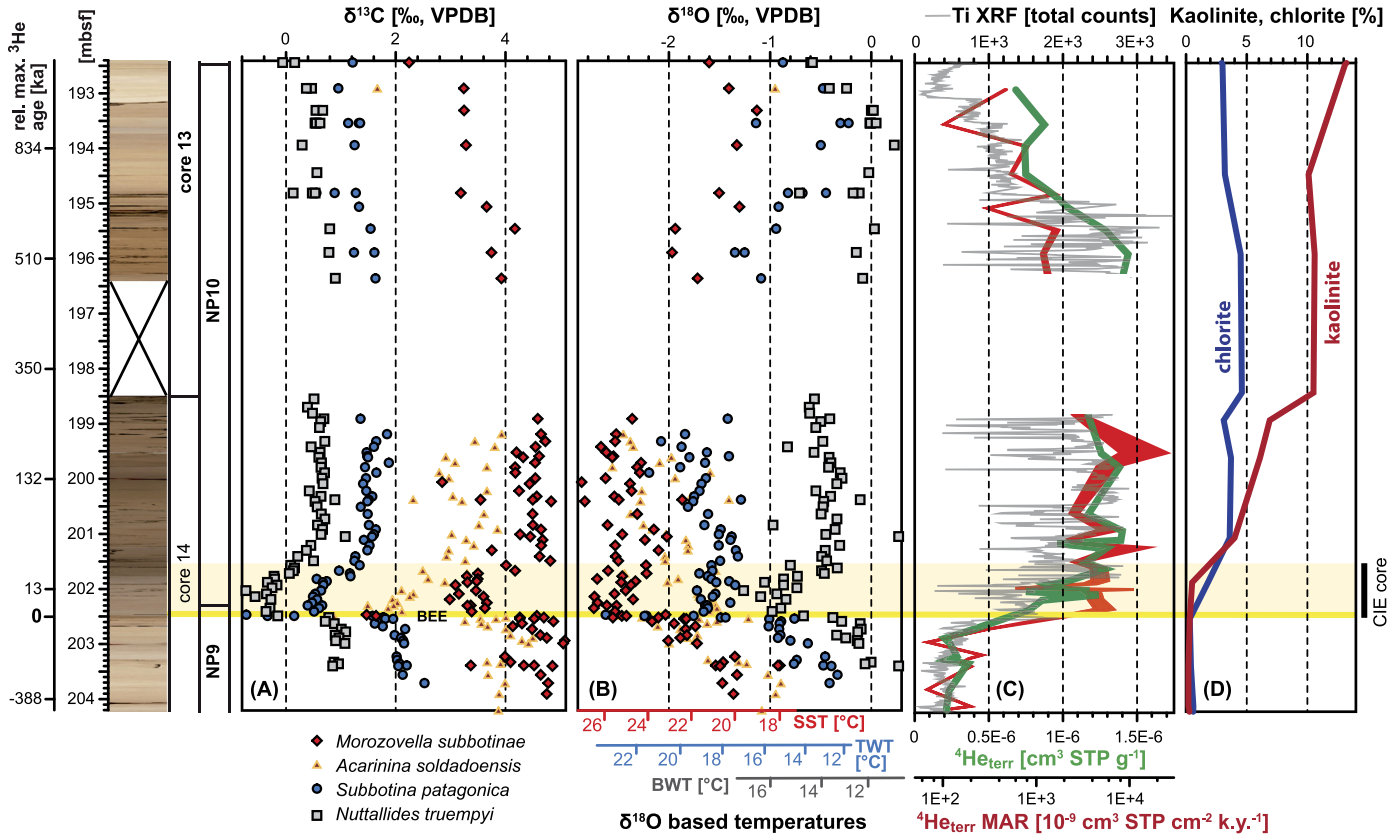

Fig. 7. Lithology, stratigraphy and geochemical data from the PETM interval at DSDP Site 401, Cores 13 and 14. (A) δ^{13}C values of foraminiferal species inhabiting different habitats (epibenthos – *Nuttallides truempyi*; thermocline dweller – *Subbotina patagonica*; surface dweller – *Morozovella subbotinae*, *Acarinina soldadoensis*). (B) δ^{18}O results of the same taxa shown in panel (A) – at the bottom of this panel are three temperature scales (SST: sea surface temperature, TWT: thermocline water temperature, BWT: bottom water temperature) assuming that the entire δ^{18}O signal can be attributed to temperature, (C) XRF core scanning Ti intensities (gray), $^4He_{terr}$ mass accumulation rates (red) and $^4He_{terr}$ concentrations [cm^3 per g sediment] (green, calculations are based on both terrestrial $^3He/^4He$ endmembers 2.1E−8 and 4E−8, and a $^3He_{ET}$ flux of 2.2E−13 cm^3 STP cm^{-2} ky^{-1}) as proxies for terrigenous input, (D) relative abundance changes of kaolinite and chlorite. Ages shown in this figure are based on Fig. 3 giving the maximum duration (in brackets) relative to the CIE onset. (For interpretation of the references to color in this figure legend, the reader is referred to the web version of this article.)

the base. However, the ambiguity of the base of the CIE at Site 401 is more likely the result of drilling disturbance rather than by carbonate dissolution. At any rate, this has no consequences for the paleoenvironmental interpretation of our data given below.

3.4. PETM temperature history ($\delta^{18}O$, Mg/Ca)

$\delta^{18}O$ data of benthic and planktic foraminifera display the typical interspecific offset between benthic foraminifera showing the heaviest $\delta^{18}O$ values, subsurface-dwellers with intermediate values, and surface-dwellers with the lightest values. The apparent difference between surface dwelling and benthic foraminifera of nearly 2‰ points towards a well-stratified water column. Below and above the clay-rich unit the difference decreases to ~1.5‰. If we attribute the entire $\delta^{18}O$ shift to temperature, bottom water temperatures would mostly be between 12 and 16 °C, thermocline waters between 12 and 22 °C and surface waters between 20 and 27 °C (Fig. 7B) with peak temperatures during the CIE core interval for all taxa. However, specifically for planktic foraminifera, it is well-known that evaporation–precipitation changes and freshwater input can alter the $\delta^{18}O$ of the surface waters and consequently the temperature estimates.

For all taxa a synchronous decrease of about 1.5‰ across the onset of the PETM has been observed, but only the benthic foraminifera record shows a distinct return to near pre-PETM $\delta^{18}O$ values at the close of the CIE core. Instead, all planktic species display a prolonged period of 'excursion-like' $\delta^{18}O$ values that persisted for several meters and, thus, throughout the $\delta^{13}C$ recovery phase and afterwards. The persistent "excursion values" of the planktic foraminifera suggest enhanced water column stratification and different histories for the near surface and bottom water-masses in the aftermath of the PETM. Based on foraminiferal $\delta^{18}O$ we can infer that either the upper water column remained warm after the PETM CIE core, or was flooded by isotopically light freshwater.

We analyzed foraminiferal Mg/Ca to test for the relative effects of changes in seawater temperature and freshwater as explanations of the persistent negative $\delta^{18}O$ signature of the post-CIE planktic foraminifera. Mg/Ca of both planktic and benthic foraminifera species suggests a warming trend of 2 and 4 °C, respectively, similar to the $\delta^{18}O$-derived relative paleotemperatures across the PETM onset (Fig. 8). The major temperature rise recorded by Mg/Ca starts prior to the PETM in the benthic foraminiferal record, but coincides with the beginning of the PETM in the two studied planktic foraminifer species (Fig. 8). The benthic foraminiferal Mg/Ca record does not recover in concert with the $\delta^{18}O$ data (Fig. 8B) suggesting no major bottom water temperature change during the CIE core and the subsequent recovery phase. This may be a consequence of a change in the intermediate-water source, with a different $\delta^{18}O$ signature during the PETM (Nunes and Norris, 2006).

While Mg/Ca in foraminiferal calcite is largely controlled by temperature (Elderfield and Ganssen, 2000; Nürnberg et al., 1996), benthic foraminiferal Mg/Ca in cold (<4 °C) environments also includes a significant influence of the carbonate saturation state ($\Delta[CO_3^{2-}]$) (Elderfield et al., 2006; Raitzsch et al., 2008; Rathmann and Kuhnert, 2008). However, we can rule out this effect, because this becomes dominant only at temperatures below 4 °C (Elderfield et al., 2006), far below bottom water temperatures we would expect for the PETM at Site 401 (>12 °C, Fig. 7B). In addition, Mg/Ca of *O. umbonatus* seem not to be influenced by $[CO_3^{2-}]$ and $\Delta[CO_3^{2-}]$ (Rathmann and Kuhnert, 2008). In contrast, low $[CO_3^{2-}]$ – as a consequence of enhanced CO_2 input during the PETM onset – can lower Mg/Ca in planktic foraminifera, since Mg is more easily removed by dissolution from the calcite crystal lattice than Ca (Regenberg et al., 2006). This could lead to an underestimation of the Mg/Ca temperatures in the upper water-column during the carbon-forcing phase of the PETM. However, diagenesis is generally unlikely to be a driving factor of Mg/Ca at Site 401, where microfossils are unusually well preserved throughout the study interval and display no indications of dissolution and recrystallization even among planktic foraminifera (Fig. 2).

We conclude that our data suggest that temperatures rose about 2–3 °C before the PETM in the deep Bay of Biscay whereas the ~1 °C increase in surface ocean temperatures was confined to the period just after the PETM onset. The observed overall magnitude of warming at Site 401 is much lower than those observed at other sites, specifically from shelf settings, the southern hemisphere and the Pacific Ocean (Sluijs et al., 2007a; Zachos et al., 2006; Zachos et al., 2003). Warming and other environmental perturbations preceding the PETM have previously been proposed for the New Jersey Margin based on palynomorphs and TEX_{86} sea-surface temperatures (Sluijs et al., 2007b), for the terrestrial Bighorn Basin in Wyoming (Secord et al., 2010) and the Egyptian shelf (Speijer and Morsi, 2002). In addition, a couple of studies suggest pre-PETM environmental change for northern Europe as discussed below, e.g. for Svalbard (Harding et al., 2011) and the North Sea area (Kender et al., 2012). The herein suggested pre-PETM switch towards warmer intermediate waters entering the North Atlantic may have contributed to the destabilization of methane hydrates ultimately leading to the PETM carbon cycle perturbation (e.g., Dickens, 2011; Dickens et al., 1995).

3.5. Evidence for enhanced freshwater input

Calculated warming inferred from planktic foraminiferal $\delta^{18}O$ exceeds Mg/Ca temperature estimates by ~3 °C on average during the clay-rich interval (Figs. 8C and 8D). The Mg/Ca-derived temperature anomaly during the PETM CIE is no more than ~1 °C for all species, whereas a negative 0.3–0.6‰ $\delta^{18}O$ shift is consistent with an inferred temperature rise between 1–3 °C in the absence of other changes in seawater $\delta^{18}O$ chemistry.

If this 0.3–0.6‰ $\delta^{18}O$ shift is actually due to seawater chemistry, this could be explained either by a change in surface ocean water masses or an increase in freshwater runoff that reduced local surface ocean salinities by 0.4–0.8 psu (analogous to the salinity-$\delta^{18}O$ gradient of modern North Atlantic surface waters, Railsback et al., 1989). Such a moderate decrease in salinity is reasonable, (i) because there are no obvious changes in the microfaunal and nannofloral assemblages indicating a substantial drop in surface-water salinity, and (ii) because of the large distance from the continents. The addition of low salinity waters is most likely, either due to enhanced run-off from the continents or due to leakage of isotopically light North Sea water (Zacke et al., 2009) into the Bay of Biscay. Alternatively, shifts in the latitudinal $\delta^{18}O$ gradients can account for this moderate $\delta^{18}O$ change, but this would neither explain the clay deposition at DSDP Site 401 nor the duration of the clay-rich unit which coincides with the $\delta^{18}O$ changes. Since both planktic foraminifera taxa *Morozovella* and *Subbotina* show a comparable offset between $\delta^{18}O$ and Mg/Ca temperatures, we have to assume that the entire mixed-layer down to the thermocline has changed its $\delta^{18}O$ composition, or alternatively that *Subbotina* was not always a thermocline indicator.

Our interpretation of enhanced run-off and stratification as reflected by the $\delta^{18}O$ decoupling of both benthic and planktic records (Fig. 7B) and the differences between $\delta^{18}O$ and Mg/Ca temperature estimates (Fig. 8) is supported by spores and dinoflagellate assemblage data from Svalbard and the North Sea Basin indicating freshening of surface waters overlying normal marine bottom waters for most of the CIE interval, but not for the PETM recovery phase (Harding et al., 2011; Kender et al., 2012). According to Kender et al. (2012) increased fluvial runoff and terrigenous input started before the CIE in the North Sea area, and may have

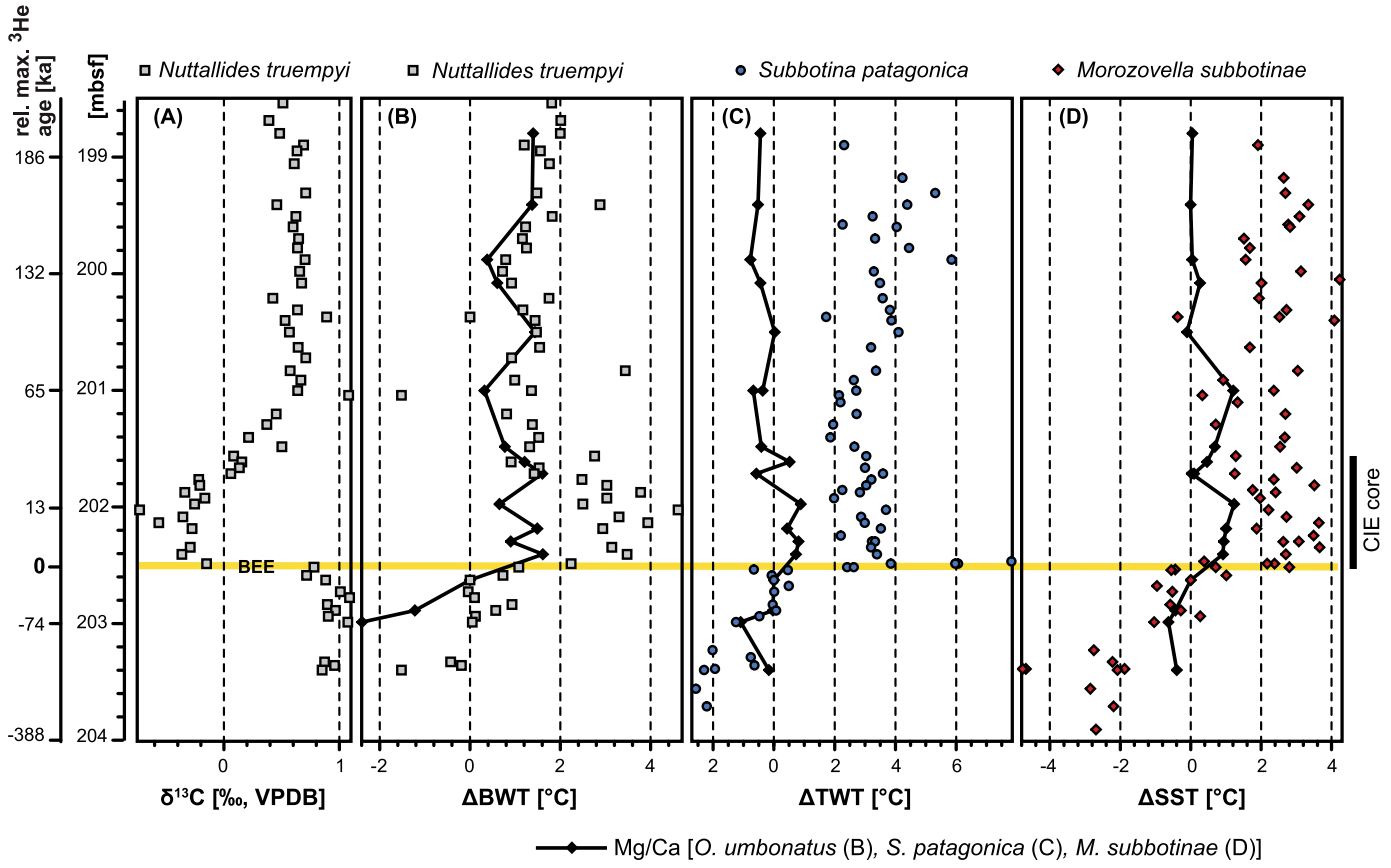

Fig. 8. Chemostratigraphy and relative temperature changes during the PETM. (A) $\delta^{13}C$ record of the benthic foraminifer *Nuttallides truempyi* for chemostratigraphy. (B–D) Relative changes of bottom water temperature (BWT, *N. truempyi*/*Oridorsalis umbonatus*), thermocline water temperature (TWT, *Subbotina patagonica*) and sea-surface temperature (SST, *Morozovella subbotinae*) in °C relative to a reference point directly below the PETM at 202.62 mbsf based on $\delta^{18}O$ (colored symbols) and Mg/Ca (black diamonds; note: for benthic foraminifera *Oridorsalis umbonatus* was analyzed instead of *N. truempyi*). Ages shown in this figure are based on Fig. 3 giving the maximum duration (in brackets) relative to the CIE onset. (For interpretation of the references to color in this figure legend, the reader is referred to the web version of this article.)

been controlled by a sea-level fall and/or tectonic activity leading to a restriction of the North Sea Basin.

3.6. Weathering and hydrological cycle

To date, severe environmental perturbations reported from other marine PETM records are stratigraphically restricted to the CIE core phase. At DSDP Site 401 we have an extended deep-sea archive of a continental response to the PETM that clearly shows that this change lasted 300–450 kyr longer than the CIE interval.

In addition to the persistent negative $\delta^{18}O$ values in the clay-rich unit, XRF core scanning derived Ti concentrations, but also Fe and Al (Figs. 4D), are consistent with a prolonged period of enhanced terrestrial input into the Bay of Biscay. Terrestrial ^{4}He MAR (Fig. 7C) increased by about an order of magnitude from pre-PETM sediments to the clay-rich (post-)PETM interval and is consistent with our clay input model (Fig. 6). Our conclusion for Site 401 also agrees with the magnitude of the increase in sedimentation rates and MAR during the PETM on the New Jersey coastal plain (John et al., 2008; Stassen et al., 2012).

In addition to the amount of terrigenous material deposited in the Bay of Biscay, XRD analyses reveal changes in the clay mineral composition during the PETM. Throughout the study interval the clay assemblage is dominated by smectite (average 64%) and illite (average 28%) (Fig. 4E). The dominance of smectite may either indicate subtropical weathering conditions with enhanced seasonality of precipitation (Thiry, 2000) or alternatively represent the alteration of basaltic oceanic crust and volcanic glasses (Chamley, 1989) such as those derived from the North Atlantic Igneous Province. Subtle changes of chlorite and kaolinite abundances have been observed within the PETM interval. Both minerals mainly increase at the expense of the relative abundance of smectite, whereas illite abundance remains relatively stable throughout the study interval (Fig. 4E). Chlorite and kaolinite are virtually absent (<1%) prior to the PETM. Chlorite appears at the onset of the PETM and makes up 4% of the clay fraction, whereas kaolinite increases steadily during the CIE recovery phase reaching 10% at the top of core 14 and nearly 15% in core 13, but does not return to lower values within the study interval (Fig. 7D). The observed patterns are similar to some sections from Spain as compiled by Schmitz and Pujalte (2003).

A kaolinite increase during the PETM has previously been reported from many places worldwide (e.g., Robert and Kennett, 1994; Knox, 1998; John et al., 2012; Kelly et al., 2005; Schmitz and Pujalte, 2003) and has usually been attributed to intensification of chemical weathering and increased erosion of older lateritic soils. However, the timing of the rise in kaolinite and its magnitude are highly variable among these records. Since it is assumed that the formation of kaolinite-bearing soils may take several hundred thousand years (Thiry, 2000), the origin of the deposited kaolinite is probably not directly linked to an increase in chemical weathering at the onset of the PETM.

Kaolinite deposited in western Europe during the PETM is considered to have been formed in the all-season warm and humid Mesozoic. During the late Paleocene to earliest Eocene, a subtropical climate with a well-marked dry season prevailed, leading

to erosion of the kaolinite during the rainy season (Thiry, 2000; Thiry and Dupuis, 2000), a similar scenario has been proposed for kaolinite on the New Jersey coastal plain (John et al., 2012). The continuous rise of kaolinite within the course of the PETM at Site 401, and the lack of a discrete pulse of kaolinite in contrast to terrestrial ^{4}He and the planktic foraminiferal δ^{18}O, suggest (i) increased erosion of kaolinite-bearing clays on the adjacent continent, and (ii) a long-term change in the source of clays associated with the onset of the PETM.

Clay deposition at DSDP Site 401 requires a source area near the Bay of Biscay. One potential source is situated in the northern part of the subtropical net-evaporation zone in western Europe, e.g., the emerged Armorican Massif (Mercier-Castiaux and Dupuis, 1990; Ziegler, 1990). Theoretically, the crystalline rocks of the Armorican Massif might provide both chlorite from metamorphic rocks and kaolinite from weathered granites, only 200 to 300 km away from DSDP Site 401. An alternative source specifically for kaolinite might be the granitic complexes in Cornwall, however, we consider the catchment area in the hinterland of Cornwall to be too small to wash sufficient clay into the Bay of Biscay to build up the clay-rich PETM succession.

The response of the hydrological cycle to the PETM has been intensively discussed and appears to be strongly dependent on the geographic position and corresponding climate zone (e.g., Pagani et al., 2006; Schmitz and Pujalte, 2007). Minor shifts in climatic belts can easily produce shifts in rainfall, vegetation and weathering systems, specifically close to 40°N (Pagani et al., 2006) across the Armorican Massif and may change the sediment supply to nearby depositional basins.

The correlation between annual rainfall and fluvial sediment transport is generally known to be poor, but maximal fluvial sediment transport takes place under dry sub-humid conditions with high seasonality (Cecil and DuLong, 2003). Maximum seasonality is reached with 3–4 wet months per year when precipitation strongly exceeds evapotranspiration. Therefore, pronounced shifts in terrestrial input and clay deposition can be related to enhanced seasonality causing maximal river discharge that may be accompanied by increased erosion during the PETM.

Our findings are in line with evidence for abrupt changes in weathering and erosion rates at the start of the PETM in southern Europe. The thick PETM succession in Zumaia (Spain) is associated with a substantial increase in clay sedimentation rate (Schmitz et al., 2001; Storme et al., 2012) as is also indicated by the thick regionally-occurring Claret conglomerate in the Pyrenees (Schmitz and Pujalte, 2007). The latter has been interpreted as mega-fan deposits caused by severe flood events due to increased precipitation and seasonality.

For North America, the picture is less ambiguous and sometimes different from western Europe. On the New Jersey Coastal Plain, sedimentation rates of fine grained siliciclastics increased by an order of magnitude during the PETM (John et al., 2008; Stassen et al., 2012). For the mid-latitudinal Bighorn Basin (Wyoming, Wing et al., 2005; Kraus and Riggins, 2007) the trend is toward more arid conditions during the PETM. For central Utah about 500 km to the south Bowen and Bowen (2008) proposed drier conditions during the PETM based on stable isotope data of paleosol nodules, and suggested a shift of precipitation from the mid-latitudes to more northern latitudes. However, this contrasts results of Retallack (2005), who calculated for Utah a substantial increase of precipitation also based on paleosol nodule analyses. Recently, Foreman et al. (2012) provided evidence that fluvial discharge in western Colorado increased substantially during the PETM and, similar to our record, for about 200 kyr afterwards. Numerical modeling results like those of Winguth et al. (2010) only partly reproduce the precipitation changes as documented in the geological climate archives from North America and western Europe.

4. Conclusions

For the PETM interval of DSDP Site 401, a ~2‰ negative δ^{13}C excursion followed by a recovery phase has been documented for all studied foraminifera taxa. Results from a dual-temperature proxy approach based on both benthic and planktic foraminiferal δ^{18}O and Mg/Ca suggest that warming in the Bay of Biscay started prior to the PETM (2–3 °C), however, the amplitude of warming across the PETM onset is smaller (~1 °C) compared to records from other regions. Starting with the onset of the CIE, a 7.5 m thick clay-rich unit was deposited and is accompanied by a $CaCO_3$ drop from 80 to 30 wt%. Calcareous microfossils from this interval show no indications of $CaCO_3$ dissolution.

We propose that the prolonged period of clay deposition at Site 401 is the result of fundamentally altered weathering conditions and changes in terrestrial sediment supply as indicated by terrestrial ^{4}He MAR, clay mineralogy and XRF core scanning. Our data support the interpretation of a 9-fold increase in terrestrial clay sedimentation during this interval, which is consistent with the observed reduction in $CaCO_3$ in absence of carbonate dissolution according to results of a numerical dilution model. Moreover, the clay-rich interval is characterized by a decoupling of benthic and planktic foraminiferal δ^{18}O as well as of planktic δ^{18}O and Mg/Ca temperatures. Both suggest enhanced input of isotopically light freshwater into the Bay of Biscay. Clay and freshwater delivery were initiated at the start of the PETM and then clearly persisted for 300–450 kyr after the end of the PETM at Site 401, thus, recording hydrologic events associated with a regional signal inside the Bay of Biscay and its hinterland. Site 401 may have been influenced by deltaic deposition or sedimentation associated with the emerged Armorican Massif.

We speculate that the climate shift, specifically enhanced hydrological cycling, associated with the PETM may have altered continental drainages or the positions of deltas, contributing to the persistence of clay sedimentation and fresh water influx long after the PETM. These new, long-lived drainage patterns were not easily reversed in the aftermath of the PETM. Alternatively, a critical climate threshold may have been surpassed in southwestern Europe at the start of the PETM that not only changed continental weathering conditions during the climatic transient, but also caused those conditions to last even after the PETM had begun to wane elsewhere. Both possible mechanisms may explain the persistent long environmental change after the climatic forcing of the PETM had stopped, contrasting with other PETM records where environmental perturbations are largely restricted to the CIE core interval.

Acknowledgements

This research used samples and data provided by the ODP. The ODP was sponsored by NSF and participating countries under the management of Joint Oceanographic Institutions (JOI). This manuscript benefited from three constructive reviews of Cedric John and two anonymous reviewers. Financial support was provided by the DFG to AB (BO2505/4-1, BO2505/5-1) and UR. RPS and SD were funded by the Research Foundation Flanders (FWO - G.0422.10) and the Research Fund KU Leuven (OT/08/018), and helium isotope analyses were partially supported by NSF grant OCE-1060877 to KAF. This research used data acquired at the XRF Core Scanner Lab at the MARUM – Center for Marine Environmental Sciences, University of Bremen.

Appendix A. Supplementary material

Supplementary material related to this article can be found online at http://dx.doi.org/10.1016/j.epsl.2014.03.017.

References

Barker, S., Greaves, M., Elderfield, H., 2003. A study of cleaning procedures used for foraminiferal Mg/Ca paleothermometry. Geochem. Geophys. Geosyst. 4. http://dx.doi.org/10.1029/2003GC000559.

Biscaye, P.E., 1965. Mineralogy and sedimentation of recent deep-sea clay in the Atlantic Ocean and adjacent seas and oceans. Geol. Soc. Am. Bull. 76, 803–832.

Bowen, G.J., Bowen, B.B., 2008. Mechanisms of PETM global change constrained by a new record from central Utah. Geology 36, 379–382.

Bowen, G.J., Beerling, D.J., Koch, P.L., Zachos, J.C., Quattlebaum, T., 2004. A humid climate state during the Palaeocene/Eocene thermal maximum. Nature 432, 495–499.

Broecker, W.S., Peng, T.-H., 1982. Tracers in the Sea. Columbia University, New York.

Cecil, C.B., DuLong, F.T., 2003. Precipitation models for sediment supply in warm climates. In: Cecil, C.B., Edgar, N.T. (Eds.), Climate Controls on Stratigraphy. SEPM, Tulsa, OK, pp. 21–27.

Chamley, H., 1989. Clay Sedimentology. Springer, Berlin.

Colosimo, A.B., Bralower, T.J., Zachos, J.C., 2006. Evidence for lysocline shoaling at the Paleocene/Eocene Thermal Maximum on Shatsky Rise. In: Northwest Pacific. Ocean Drill. Program Proc., Sci. Results, vol. 198. Ms 198SR-112.

Cramer, B.S., Wright, J.D., Kent, D.V., Aubry, M.P., 2003. Orbital climate forcing of δ^{13}C excursions in the late Paleocene–early Eocene (chrons C24n–C25n). Paleoceanography 18. http://dx.doi.org/10.1029/2003PA000909.

D'haenens, S., Bornemann, A., Stassen, P., Speijer, R.P., 2012. Multiple early Eocene benthic foraminiferal assemblage and δ^{13}C fluctuations at DSDP Site 401 (Bay of Biscay – NE Atlantic). Mar. Micropaleontol. 88–89, 15–35.

DeConto, R.M., Galeotti, S., Pagani, M., Tracy, D., Schaefer, K., Zhang, T., Pollard, D., Beerling, D.J., 2012. Past extreme warming events linked to massive carbon release from thawing permafrost. Nature 484, 87–91.

Dickens, G.R., 2011. Down the Rabbit Hole: toward appropriate discussion of methane release from gas hydrate systems during the Paleocene–Eocene thermal maximum and other past hyperthermal events. Clim. Past 7, 831–846.

Dickens, G.R., O'Neil, J.R., Rea, D.K., Owen, R.M., 1995. Dissociation of oceanic methane hydrate as a cause of the carbon-isotope excursion at the end of the Paleocene. Paleoceanography 10, 965–971.

Dypvik, H., Riber, L., Burca, F., Rüther, D., Jargvoll, D., Nagy, J., Jochmann, M., 2011. The Paleocene–Eocene thermal maximum (PETM) in Svalbard – clay mineral and geochemical signals. Palaeogeogr. Palaeoclimatol. Palaeoecol. 302, 156–169.

Edgar, K.M., Bohaty, S.M., Gibbs, S.J., Sexton, P.F., Norris, R.D., Wilson, P.A., 2012. Symbiont 'bleaching' in planktic foraminifera during the Middle Eocene Climatic Optimum. Geology 41, 15–18.

Ehrmann, W.U., Melles, M., Kuhn, G., Grobe, H., 1992. Significance of clay mineral assemblages in the Antarctic Ocean. Mar. Geol. 107, 249–273.

Elderfield, H., Ganssen, G., 2000. Past temperature and δ^{18}O of surface ocean waters inferred from foraminiferal Mg/Ca ratios. Nature 405, 442–445.

Elderfield, H., Yu, J., Anand, P., Kiefer, T., Nyland, B., 2006. Calibrations for benthic foraminiferal Mg/Ca paleothermometry and the carbonate ion hypothesis. Earth Planet. Sci. Lett. 250, 633–649.

Erez, J., Luz, B., 1982. Temperature control of oxygen-isotope fractionation of cultured planktonic-foraminifera. Nature 297, 220–222.

Farley, K.A., 1995. Cenozoic variations in the flux of interplanetary dust recorded by He-3 in a deep-sea sediment. Nature 376, 153–156.

Farley, K.A., Eltgroth, S.F., 2003. An alternative age model for the Paleocene–Eocene thermal maximum using extraterrestrial ^{3}He. Earth Planet. Sci. Lett. 208, 135–148.

Farley, K.A., Mukhopadhyay, S., 2001. An extraterrestrial impact at the Permian–Triassic boundary?. Science 293, 2343a.

Foreman, B.Z., Heller, P.L., Clementz, M.T., 2012. Fluvial response to abrupt global warming at the Palaeocene/Eocene boundary. Nature 491, 92–95.

Gibbs, S.J., Bown, P.R., Sessa, J.A., Bralower, T.J., Wilson, P.A., 2006. Nannoplankton extinction and origination across the Paleocene–Eocene Thermal Maximum. Science 314, 1770–1773.

Giusberti, L., Rio, D., Agnini, C., Backman, J., Fornaciari, E., Tateo, F., Oddone, M., 2007. Mode and tempo of the Paleocene–Eocene thermal maximum in an expanded section from the Venetian pre-Alps. Geol. Soc. Am. Bull. 119, 391–412.

Harding, I.C., Charles, A.J., Marshall, J.E.A., Pälike, H., Roberts, A.P., Wilson, P.A., Jarvis, E., Thorne, R., Morris, E., Moremon, R., Pearce, R.B., Akbari, S., 2011. Sea-level and salinity fluctuations during the Paleocene–Eocene thermal maximum in Arctic Spitsbergen. Earth Planet. Sci. Lett. 303, 97–107.

Huber, M., Sloan, L., Shellito, C., 2003. Early Paleogene oceans and climate: a fully coupled modeling approach using the NCAR CSM. In: Wing, S.L., Gingerich, P.D., Schmitz, B., Thomas, E. (Eds.), Causes and Consequences of Globally Warm Climates in the Early Paleogene, pp. 25–47.

John, C.M., Bohaty, S.M., Zachos, J.C., Sluijs, A., Gibbs, S., Brinkhuis, H., Bralower, T.J., 2008. North American continental margin records of the Paleocene–Eocene thermal maximum: implications for global carbon and hydrological cycling. Paleoceanography 23, 1–20.

John, C.M., Banerjee, N.R., Longstaffe, F.J., Sica, C., Law, K.R., Zachos, J.C., 2012. Clay assemblage and oxygen isotopic constraints on the weathering response to the Paleocene–Eocene thermal maximum, east coast of North America. Geology 40, 591–594.

Kelly, D.C., Bralower, T.J., Zachos, J.C., Silva, I.P., Thomas, E., 1996. Rapid diversification of planktonic foraminifera in the tropical Pacific (ODP Site 865) during the late Paleocene thermal maximum. Geology 24, 423–426.

Kelly, D.C., Zachos, J.C., Bralower, T.J., Schellenberg, S.A., 2005. Enhanced terrestrial weathering/runoff and surface ocean carbonate production during the recovery stages of the Paleocene–Eocene thermal maximum. Paleoceanography 20. http://dx.doi.org/10.1029/2005PA001163.

Kender, S., Stephenson, M.H., Riding, J.B., Leng, M.J., Knox, R.W.O.B., Peck, V.L., Kendrick, C.P., Ellis, M.A., Vane, C.H., Jamieson, R., 2012. Marine and terrestrial environmental changes in NW Europe preceding carbon release at the Paleocene–Eocene transition. Earth Planet. Sci. Lett. 353–354, 108–120.

Kennett, J.P., Stott, L.D., 1991. Abrupt deep-sea warming, palaeoceanographic changes and benthic extinctions at the end of the Paleocene. Nature 353, 225–229.

Knox, R.W.O., 1985. Stratigraphic significance of volcanic ash in Paleocene and Eocene sediments at Sites 549 and 550. Init. Rep. Deep-Sea Drill. Proj. 80, 845–850.

Knox, R.W.O.B., 1998. Kaolinite influx within Paleocene/Eocene boundary strata of western Europe. Newsl. Stratigr. 36, 49–53.

Komar, N., Zeebe, R.E., 2011. Oceanic calcium changes from enhanced weathering during the Paleocene–Eocene thermal maximum: no effect on calcium-based proxies. Paleoceanography 26. http://dx.doi.org/10.1029/2010pa001979.

Kraus, M.J., Riggins, S., 2007. Transient drying during the Paleocene–Eocene Thermal Maximum (PETM): analysis of paleosols in the Bighorn Basin, Wyoming. Palaeogeogr. Palaeoclimatol. Palaeoecol. 245, 444–461.

Kroopnick, P.M., 1985. The distribution of ^{13}C of ΔCO_2 in the world oceans. Deep-Sea Res. 32, 57–84.

Lear, C.H., Elderfield, H., Wilson, P.A., 2000. Cenozoic deep-sea temperatures and global ice volumes from Mg/Ca in benthic foraminiferal calcite. Science 287, 269–272.

Lunt, D.J., Valdes, P.J., Jones, T.D., Ridgwell, A., Haywood, A.M., Schmidt, D.N., Marsh, R., Maslin, M., 2010. CO_2-driven ocean circulation changes as an amplifier of Paleocene–Eocene thermal maximum hydrate destabilization. Geology 38, 875–878.

Marcantonio, F., Thomas, D.J., Woodard, S., McGee, D., Winckler, G., 2009. Extraterrestrial ^{3}He in Paleocene sediments from Shatsky Rise: constraints on sedimentation rate variability. Earth Planet. Sci. Lett. 287, 24–30.

McCarren, H., Thomas, E., Hasegawa, T., Röhl, U., Zachos, J.C., 2008. Depth dependency of the Paleocene–Eocene carbon isotope excursion: paired benthic and terrestrial biomarker records (Ocean Drilling Program Leg 208, Walvis Ridge). Geochem. Geophys. Geosyst. 9. http://dx.doi.org/10.1029/2008GC002116.

McInerney, F.A., Wing, S.L., 2011. The Paleocene–Eocene Thermal Maximum: a perturbation of carbon cycle, climate, and biosphere with implications for the future. Annu. Rev. Earth Planet. Sci. 39, 489–516.

Mercier-Castiaux, M., Dupuis, C., 1990. Clay mineral associations in the Ypresian Formations in the NW European Basin. Time and geographical variations—interpretations. Bull. Soc. Belge Géol. 97, 441–450.

Montadert, L., et al., 1979. (DSDP) Site 401. Initial reports of the Deep Sea Drilling Project, Leg 48, in: Brest, France to Aberdeen, Scotland, 1976. Init. Res. Deep-Sea Drill. Proj. 48, 73–124.

Mukhopadhyay, S., Farley, K.A., Montanari, A., 2001. A short duration of the Cretaceous–Tertiary boundary event: evidence from extraterrestrial helium-3. Science 291, 1952–1955.

Müller, G., Gastner, M., 1971. The "Karbonat-Bombe", a simple device for the determination of the carbonate content in sediments, soils, and other materials. Neues Jahrb. Mineral., Monatsh. 10, 466–469.

Murphy, B.H., Farley, K.A., Zachos, J.C., 2010. An extraterrestrial ^{3}He-based timescale for the Paleocene–Eocene thermal maximum (PETM) from Walvis Ridge, IODP Site 1266. Geochim. Cosmochim. Acta 74, 5098–5108.

Norris, R.D., 1996. Symbiosis as an evolutionary innovation in the radiation of Paleocene planktic foraminifera. Paleobiology 22, 461–480.

Nunes, F., Norris, R.D., 2006. Abrupt reversal in ocean overturning during the Palaeocene/Eocene warm period. Nature 439, 60–63.

Nürnberg, D., Bijma, J., Hemleben, C., 1996. Assessing the reliability of magnesium in foraminiferal calcite as a proxy for water mass temperatures. Geochim. Cosmochim. Acta 60, 803–814.

Pagani, M., Pedentchouk, N., Huber, M., Sluijs, A., Schouten, S., Brinkhuis, H., Damste, J.S.S., Dickens, G.R., Scientists, E., 2006. Arctic hydrology during global warming at the Palaeocene/Eocene thermal maximum. Nature 442, 671–675.

Patterson, D.B., Farley, K.A., 1998. Extraterrestrial ^{3}He in seafloor sediments: evidence for correlated 100 kyr periodicity in the accretion rate of interplanetary dust, orbital parameters, and Quaternary climate. Geochim. Cosmochim. Acta 62, 3669–3682.

Petschick, R., Kuhn, G., Gingele, F., 1996. Clay mineral distribution in surface sediments of the South atlantic: sources, transport, and relation to oceanography. Mar. Geol. 130, 203–229.

Raffi, I., Backman, J., Palike, H., 2005. Changes in calcareous nannofossil assemblages across the Paleocene/Eocene transition from the paleo-equatorial Pacific Ocean. Palaeogeogr. Palaeoclimatol. Palaeoecol. 226, 93–126.

Railsback, L.B., Anderson, T.F., Ackerly, S.C., Cisne, J.L., 1989. Paleoceanographic modeling of temperature–salinity profiles from stable isotopic data. Paleoceanography 4, 585–591.

Raitzsch, M., Kuhnert, H., Groeneveld, J., Bickert, T., 2008. Benthic foraminifer Mg/Ca anomalies in South Atlantic core top sediments and their implications for paleothermometry. Geochem. Geophys. Geosyst. 9. http://dx.doi.org/10.1029/2007GC001788.

Rathmann, S., Kuhnert, H., 2008. Carbonate ion effect on Mg/Ca, Sr/Ca and stable isotopes on the benthic foraminifera *Oridorsalis umbonatus* off Namibia. Mar. Micropaleontol. 66, 120–133.

Regenberg, M., Nurnberg, D., Steph, S., Groeneveld, J., Garbe-Schonberg, D., Tiedemann, R., Dullo, W.C., 2006. Assessing the effect of dissolution on planktonic foraminiferal Mg/Ca ratios: evidence from Caribbean core tops. Geochem. Geophys. Geosyst. 7. http://dx.doi.org/10.1029/2005GC001019.

Retallack, G.J., 2005. Pedogenic carbonate proxies for amount and seasonality of precipitation in paleosols. Geology 33, 333–336.

Ridgwell, A., Schmidt, D.N., 2010. Past constraints on the vulnerability of marine calcifiers to massive carbon dioxide release. Nat. Geosci. 3, 196–200.

Robert, C., Kennett, J.P., 1994. Antarctic subtropical humid episode at the Paleocene–Eocene boundary — clay-mineral evidence. Geology 22, 211–214.

Röhl, U., Westerhold, T., Bralower, T.J., Zachos, J.C., 2007. On the duration of the Paleocene–Eocene thermal maximum (PETM). Geochem. Geophys. Geosyst. 8. http://dx.doi.org/10.1029/2007GC001784.

Schmitz, B., Pujalte, V., 2003. Sea-level, humidity, and land-erosion records across the initial Eocene thermal maximum from a continental–marine transect in northern Spain. Geology 31, 689.

Schmitz, B., Pujalte, V., 2007. Abrupt increase in seasonal extreme precipitation at the Paleocene–Eocene boundary. Geology 35, 215–218.

Schmitz, B., Pujalte, V., Nunez-Betelu, K., 2001. Climate and sea-level perturbations during the initial Eocene thermal maximum: evidence from siliciclastic units in the Basque Basin (Ermua Zumaia and Trabakua Pass), northern Spain. Palaeogeogr. Palaeoclimatol. Palaeoecol. 165, 299–320.

Secord, R., Gingerich, P.D., Lohmann, K.C., MacLeod, K.G., 2010. Continental warming preceding the Palaeocene–Eocene Thermal Maximum. Nature 467, 955–958.

Shackleton, N.J., 1974. Attainment of isotopic equilibrium between ocean water and the benthonic foraminifera genus *Uvigerina* – isotopic changes in the ocean during the last glacial. In: Labeyrie, L. (Ed.), Colloquium CNRS, pp. 203–209.

Sluijs, A., Bowen, G.J., Brinkhuis, H., Lourens, L.J., Thomas, E., 2007a. The Palaeocene–Eocene Thermal Maximum super greenhouse: biotic and geochemical signatures, age models and mechanisms of global change. In: Williams, M., Haywood, A.M., Gregory, F.J., Schmidt, D.N. (Eds.), Deep-Time Perspectives on Climate Change - Marrying the Signal from Computer Models and Biological Proxies. Geological Society, London, pp. 323–349.

Sluijs, A., Brinkhuis, H., Schouten, S., Bohaty, S.M., John, C.M., Zachos, J.C., Reichart, G.J., Damste, J.S.S., Crouch, E.M., Dickens, G.R., 2007b. Environmental precursors to rapid light carbon injection at the Palaeocene/Eocene boundary. Nature 450, 1218–1221.

Speijer, R.P., Morsi, A.M.M., 2002. Ostracode turnover and sea-level changes associated with the Paleocene–Eocene thermal maximum. Geology 30, 23–26.

Speijer, R.P., Scheibner, C., Stassen, P., Morsi, A.M.M., 2012. Response of marine ecosystems to deep-time global warming: a synthesis of biotic patterns across the Paleocene–Eocene Thermal Maximum (PETM). Austrian J. Earth Sci. 105, 6–16.

Stassen, P., Thomas, E., Speijer, R.P., 2012. Integrated stratigraphy of the Paleocene–Eocene thermal maximum in the New Jersey Coastal Plain: toward understanding the effects of global warming in a shelf environment. Paleoceanography 27. http://dx.doi.org/10.1029/2012PA002323.

Storme, J.-Y., Devleeschouwer, X., Schnyder, J., Cambier, G., Baceta, J.I., Pujalte, V., Di Matteo, A., Iacumin, P., Yans, J., 2012. The Palaeocene/Eocene boundary section at Zumaia (Basque–Cantabric Basin) revisited: new insights from high-resolution magnetic susceptibility and carbon isotope chemostratigraphy on organic matter ($\delta^{13}C_{org}$). Terra Nova 24, 310–317.

Svensen, H., Planke, S., Malthe-Sorenssen, A., Jamtveit, B., Myklebust, R., Eidem, T.R., Rey, S.S., 2004. Release of methane from a volcanic basin as a mechanism for initial Eocene global warming. Nature 429, 542–545.

Thiry, M., 2000. Palaeoclimatic interpretation of clay minerals in marine deposits: an outlook from the continental origin. Earth-Sci. Rev. 49, 201–221.

Thiry, M., Dupuis, C., 2000. Use of clay minerals for paleoclimatic reconstructions; limits of the method with special reference to the Paleocene–lower Eocene interval. GFF 122, 166–167.

Thomas, E., 2007. Cenozoic mass extinctions in the deep sea: what perturbs the largest habitat on Earth?. Geol. Soc. Am. Spec. Paper 424, pp. 1–23.

Tindall, J., Flecker, R., Valdes, P., Schmidt, D.N., Markwick, P., Harris, J., 2010. Modelling the oxygen isotope distribution of ancient seawater using a coupled ocean–atmosphere GCM: implications for reconstructing early Eocene climate. Earth Planet. Sci. Lett. 292, 265–273.

Tripati, A., Elderfield, H., 2005. Deep-sea temperature and circulation changes at the Paleocene–Eocene thermal maximum. Science 308, 1894–1898.

Vandenberghe, N., Hilgen, F.J., Speijer, R.P., 2012. The Paleogene Period. In: Gradstein, F.M., Ogg, J.G., Schmitz, M., Ogg, G. (Eds.), A Geologic Time Scale 2012. Elsevier, pp. 855–921.

Westerhold, T., Röhl, U., 2009. High resolution cyclostratigraphy of the early Eocene – new insights into the origin of the Cenozoic cooling trend. Clim. Past 5, 309–327.

Wing, S.L., Harrington, G.J., Smith, F.A., Bloch, J.I., Boyer, D.M., Freeman, K.H., 2005. Transient floral change and rapid global warming at the Paleocene–Eocene boundary. Science 310, 993–996.

Winguth, A., Shellito, C., Shields, C., Winguth, C., 2010. Climate response at the Paleocene–Eocene Thermal Maximum to greenhouse gas forcing – A model study with CCSM3. J. Climate 23, 2562–2584.

Winguth, A.M.E., Thomas, E., Winguth, C., 2012. Global decline in ocean ventilation, oxygenation, and productivity during the Paleocene–Eocene Thermal Maximum: implications for the benthic extinction. Geology 40, 263–266.

Zachos, J.C., McCarren, H., Murphy, B., Röhl, U., Westerhold, T., 2010. Tempo and scale of late Paleocene and early Eocene carbon isotope cycles: implications for the origin of hyperthermals. Earth Planet. Sci. Lett. 299, 242–249.

Zachos, J.C., Röhl, U., Schellenberg, S.A., Sluijs, A., Hodell, D.A., Kelly, D.C., Thomas, E., Nicolo, M., Raffi, I., Lourens, L.J., McCarren, H., Kroon, D., 2005. Rapid acidification of the ocean during the Paleocene–Eocene thermal maximum. Science 308, 1611–1615.

Zachos, J.C., Schouten, S., Bohaty, S., Quattlebaum, T., Sluijs, A., Brinkhuis, H., Gibbs, S.J., Bralower, T.J., 2006. Extreme warming of mid-latitude coastal ocean during the Paleocene–Eocene Thermal Maximum: inferences from TEX_{86} and isotope data. Geology 34, 737–740.

Zachos, J.C., Stott, L.D., Lohmann, K.C., 1994. Evolution of early Cenozoic marine temperatures. Paleoceanography 9, 353–387.

Zachos, J.C., Wara, M.W., Bohaty, S., Delaney, M.L., Petrizzo, M.R., Brill, A., Bralower, T.J., Premoli-Silva, I., 2003. A transient rise in tropical sea surface temperature during the Paleocene–Eocene Thermal Maximum. Science 302, 1551–1554.

Zacke, A., Voigt, S., Joachimski, M.M., Gale, A.S., Ward, D.J., Tütken, T., 2009. Surface-water freshening and high-latitude river discharge in the Eocene North Sea. J. Geol. Soc. 166, 969–980.

Zeebe, R.E., Zachos, J.C., 2007. Reversed deep-sea carbonate ion basin gradient during Paleocene–Eocene thermal maximum. Paleoceanography 22. http://dx.doi.org/10.1029/2006PA001395.

Ziegler, P.A., 1990. Geological Atlas of Western and Central Europe, 2nd and completely rev. ed. Shell Internationale Petroleum Maatschappij B.V., The Hague.